

**=enter title here=**

**=list all authors here=**

**=number= =Affiliation Address=**

**4 Key Points:**

- 5** • enter point 1 here  
**6** • enter point 2 here  
**7** • enter point 3 here

---

Corresponding author: =name=, =email address=

8      **Abstract**  
 9      enter abstract here

10     **1 Introduction**

11    Slow slip events are a new feature discovered in the last two decades in many sub-  
 12    duction zones thanks to recordings of the displacement of Earth's surface by dense Global  
 13    Navigation Satellite System (GNSS) networks. As with ordinary earthquakes, slow slip  
 14    events are caused by slip on a fault, such as the plate boundary between a tectonic plate  
 15    subducting under another tectonic plate. However, they take a much longer time (sev-  
 16    eral days to several years) to happen relative to ordinary earthquakes, and they have a  
 17    relatively short recurrence time (months to years), compared to the recurrence time of  
 18    regular earthquakes (up to several hundreds of years), allowing scientists to observe and  
 19    study many complete event cycles, which is typically not possible to explore with tra-  
 20    ditional earthquake catalogs (Beroza & Ide, 2011). A slow slip event on the plate bound-  
 21    ary is inferred to happen when there is a reversal of the direction of motion at GNSS sta-  
 22    tions, compared to the secular interseismic motion. Slow slip events have been observed  
 23    in many subduction zones, such as Cascadia, Nankai (southwest Japan), Alaska, Costa  
 24    Rica, Mexico, and New Zealand (Audet & Kim, 2016; Beroza & Ide, 2011).

25    In many places, tectonic tremor are also observed in relation to slow slip. Tremor  
 26    is a long (several seconds to many minutes), low amplitude seismic signal, with emer-  
 27    gent onsets, and an absence of clear impulsive phases. Tectonic tremor have been explained  
 28    as a swarm of small, low-frequency earthquakes (LFEs) (Shelly, Beroza, & Ide, 2007),  
 29    that is small magnitude earthquakes ( $M \sim 1$ ), for which frequency content (1-10 Hz) is  
 30    lower than for ordinary earthquakes (up to 20 Hz). In subduction zones such as Nankai  
 31    and Cascadia, tectonic tremor observations are spatially and temporally correlated with  
 32    slow slip observations (Obara, 2002; Rogers & Dragert, 2003). Due to this correlation,  
 33    these paired phenomena have been called Episodic Tremor and Slip (ETS). However, this  
 34    is not always the case. For instance, in northern New Zealand, tremor are more challeng-  
 35    ing to detect, and seem to be located downdip of the slow slip on the plate boundary.

36    In Cascadia and Guerrero, Mexico, tremor has been used as a proxy to observe slow  
 37    slip events that are not directly detectable in the GNSS data. For instance, Aguiar, Mel-  
 38    bourne, and Scrivner (2009) computed the GPS-estimated moment release for 23 ETS  
 39    events in Cascadia between 1997 and 2008. Simultaneously, they computed the cumu-  
 40    lative number of hours of tectonic tremor recorded for each event. They observed a lin-  
 41    ear relationship between moment release and number of hours of tremor for ETS events  
 42    of moment magnitude 6.3 to 6.8. For all these events, at least 50 hours of tectonic tremor  
 43    where observed simultaneously with the GPS deformation. However, many smaller bursts  
 44    of tremor of duration 1 to 50 hours were also observed in between the big ETS events.  
 45    Based on the relationship between slow slip moment and number of hours of tremor, Aguiar  
 46    et al. (2009) suggested that smaller slow slip events of magnitude 5-6 may occur sim-  
 47    taneously with the tremor bursts without being detectable in the GPS data.

48    Frank (2016) transformed the GPS time series into daily increments of surface mo-  
 49    tion by computing the first order differentiation of the time series. He then discarded  
 50    the daily increments observed during known big slow slip events, and focused on the inter-  
 51    events period. He divided the daily increments into two groups: the first group contains  
 52    days when slow seismicity (tectonic tremor and LFEs) is detected, the second group con-  
 53    tains days when the numbers of LFEs (for Guerrero) or tremor (for Cascadia) is lower  
 54    than a threshold. He then stacked separately the two groups of daily increments and ob-  
 55    served a cumulative displacement in the northern direction (for Guerrero) and the east-  
 56    ern direction (for Cascadia) corresponding to the loading period when few tremor or LFEs  
 57    are observed and the surface deformation corresponds to the secular plate motion. He  
 58    also observed a cumulative displacement in the southern direction (for Guerrero) and  
 59    the western direction (for Cascadia) corresponding to the release period when tremor

60 and LFEs are observed. This reverse displacement corresponds to smaller slow slip events  
61 not directly observable in the GPS data.

62 However, in other subduction zones such as New Zealand, there is no clear rela-  
63 tionship between tremor and slow slip occurrence and these methods cannot be applied.  
64 We thus need other methods to be able to better detect and quantify slow slip.

65 Wavelets methods such as the Discrete Wavelet Transform (DWT) are mathemat-  
66 ical tools for analyzing time series simultaneously in the time and the frequency domain  
67 by observing how weighted averages of a time series vary from one averaging period to  
68 the next. Wavelet methods have been widely used for geophysical applications (Kumar  
69 & Foufoula-Georgiou, 1997). However, few studies have used wavelet methods to ana-  
70 lyze recordings of slow slip, and their scope was limited to the detection of the bigger  
71 (magnitude 6-7) short-term (a few weeks) events. **Add references**

72 Alba, Weldon, Livelybrooks, and Schmidt (2019) used hourly water level records  
73 from four tide gauges in the Juan de Fuca Straight and the Puget Sound to determine  
74 vertical displacements, uplift rates between ETS events, and net uplift rates between 1996  
75 and 2011. The noise in the tide gauges data is associated with tides, and ocean and at-  
76 mospheric noise on multiple timescales (a few days for storms to decades for oscillations  
77 between ocean basins), and is assumed to be coherent between each of the four tidal gauges  
78 studied. On the contrary, the uplift due to ETS events should be different at each tidal  
79 gauge. They first removed the tides using NOAA hourly harmonic tidal predictions. They  
80 then removed the residual noise using a method based on the DWT. More precisely, the  
81 authors applied a DWT to each of the four sites studied, and to the average of the four  
82 sites. Then, for each level of the DWT decomposition, they carried out a linear regres-  
83 sion between the detail for one site and the detail for the average of the four sites. This  
84 process gives a coefficient for each level and for each site. They then constructed a noise  
85 signal for each site by multiplying the coefficient from the linear regression by the de-  
86 tail of the average over the four sites, and summing for all levels. The noise signal thus  
87 obtained was then removed from the time series. They then stacked multiple events to  
88 obtain an average event uplift rate, aligning the 12 ETS events using exact timing from  
89 GPS data. A difference in uplift between the two tidal gauges at Port Angeles and Port  
90 Townsend was then clearly seen in the stacked time series. Finally, the authors removed  
91 the long-term uplift rate and the long-term sea level rise to obtain an average inter-event  
92 uplift rate. They found that the inter-event deformation at a site is equal and opposite  
93 to the deformation during an ETS event, suggesting that ETS events are, on average,  
94 releasing the strain accumulated between ETS events.

95 Szeliga, Melbourne, Santillan, and Miller (2008) determined the timing and the  
96 amplitude of 34 slow slip events throughout the Cascadia subduction zone between 1997  
97 and 2005. They stabilized the GPS time series using a reference set of stations from sta-  
98 ble North America. They then modelled the GPS time series by the sum of a linear trend,  
99 annual and biannual sinusoids representing seasonal effects, and Heaviside step functions  
100 corresponding to earthquakes and hardware upgrades. The linear system was then solved  
101 using a weighted QR decomposition. Finally, they applied a Gaussian wavelet transform  
102 to the residual time series to get the exact timing of the slow slip at each GPS station.  
103 The succeeding wavelet basis functions are increasingly sensitive to temporal localiza-  
104 tion of a given signal, and the onset of faulting appears on the wavelet spectrum as an  
105 amplitude spike present over all frequencies. The offset for each slow slip event was then  
106 used to invert for the slow slip at depth by assuming a thrust fault slip at each subfault  
107 of the plate boundary. An equivalent moment magnitude was thus obtained.

108 Finally, instead of using wavelets in the time domain, Ohtani, McGuire, and Segall  
109 (2010) used 2D wavelet functions in the spatial domain to detect slow slip events. They  
110 designed the Network Stain Filter (NSF) to detect transient deformation signals from  
111 large-scale geodetic arrays. Contrary to their previous work on the Network Inversion  
112 Filter (NIF), there is no need to specify potential sources of deformation. They mod-  
113 elled the position of the GPS station by the sum of the secular velocity, a spatially co-  
114 herent field, site-specific noise, reference frame errors, and observation errors. The spa-

**Strait of Juan de**

115 tial displacement field is modeled by the sum of basis wavelets (the Deslauriers-Dubuc  
 116 wavelet of degree 3) with time-varying weights. The transient is considered to be nearly  
 117 steady-state, so that it has spatial weights for the displacement and the velocity, but the  
 118 acceleration is modeled by a random walk with a time-varying variance. All the time varying  
 119 coefficients are estimated using Kalman filtering, and the optimization problem is  
 120 regularized with the spatial sum of the transient strain rate field. Their method has been  
 121 successfully used to detect a transient event in the Boso peninsula, Japan, and a slow  
 122 slip event in the Alaska subduction zone (Wei, McGuire, & Richardson, 2012).

123 In this study, we use wavelet methods to analyze GPS and seismic recordings of  
 124 slow slip events in Cascadia. Our objective is to verify that there is a good correlation  
 125 between slow slip events detected with only GNSS data, and slow slip events detected  
 126 with only seismic data. We thus want to demonstrate that the wavelet-based detection  
 127 method can be applied to detect slow slip events that may be currently undetected with  
 128 standard methods.

**State how many new SSEs we have detected.**

## 129 2 Data

130 We focused our study on northwest Washington State. For the GNSS data, we used  
 131 the GPS time series provided by the Pacific Northwest Geodetic Array, Central Wash-  
 132 ington University. These are network solutions in ITRF2008 with phase ambiguities re-  
 133 solved. Solutions are computed with JPL/NASA orbits and satellite clocks. North, East,  
 134 and Vertical directions are available. However, as the direction of the secular plate mo-  
 135 tion is close to the East direction, we only used the East direction of the GPS time se-  
 136 ries for the data analysis, as it has the best signal-to-noise ratio. The wavelet method  
 137 works best with data with zero mean, and no sharp discontinuities, so we use the cleaned  
 138 dataset, that is GPS times eries with linear trends, steps due to earthquakes or hard-  
 139 ware upgrades, and annual and semi-annual sinusoids signals simultaneously estimated  
 140 and removed following Szeliga, Melbourne, Miller, and Santillan (2004). For the seis-  
 141 mic data, we used the tremor catalog from the Pacific Northwest Seismic Network (PNSN)  
 142 (Wech, 2010). Tremor were detected and located using waveform envelope correlation  
 143 and clustering and a centroid location is available for every given five-minute time win-  
 144 dow when tremor was detected. As the catalog starts in August 2009, we only looked  
 145 at GPS data recorded in 2009 or later.

**For the area you are analyzing the tremor catalog goes back to  
 January 2007**

## 146 3 Method

### 147 3.1 The Maximal Overlap Discrete Wavelet Transform

148 The Discrete Wavelet Transform (DWT) is an orthonormal transform that trans-  
 149 forms a time series  $X_t$  ( $t = 0, \dots, N - 1$ ) into a vector of wavelet coefficients  $W_i$  ( $i = 0, \dots, N - 1$ ).  
 150 If we denote  $J$  the level of the wavelet decomposition, and we have  $N = n*2^J$ , where  
 151  $n$  is some integer higher or equal to 1, the vector of wavelet coefficients can be decom-  
 152 posed into  $J$  wavelet vectors  $W_j$  of lengths  $\frac{N}{2}, \frac{N}{4}, \dots, \frac{N}{2^J}$ , and one scaling vector  $V_J$  of  
 153 length  $\frac{N}{2^J}$ . Each wavelet vector  $W_j$  is associated with changes on scale  $\tau_j = dt2^{j-1}$ , where  
 154  $dt$  is the time step of the time series, and corresponds to the filtering of the original time  
 155 series with a filter with nominal frequency interval  $[\frac{1}{dt2^{j+1}}, \frac{1}{dt2^j}]$ . The scaling vector  $V_J$   
 156 is associated with averages in scale  $\lambda_J = dt2^J$ , and corresponds to the filtering of the  
 157 original time series with a filter with nominal frequency interval  $[0, \frac{1}{dt2^{j+1}}]$ . We can also  
 158 define for  $j = 1, \dots, J$  the  $j$ th wavelet detail  $D_j$ , which is a vector of length  $N$ , and  
 159 is associated to scale  $\tau_j = dt2^{j-1}$ . Similarly, we can define for  $j = 1, \dots, J$  the  $j$ th  
 160 wavelet smooth  $S_j$ , which is a vector of length  $N$ , and is associated to scales  $\tau_{j+1} = dt2^{j+1}$   
 161 and higher. Together, the details and the smooths define the multiresolution analysis (MRA)  
 162 of  $X$ :

$$X = \sum_{j=1}^J D_j + S_J \quad (1)$$

The DWT present several disadvantages. First, the length of the time series must be a multiple of  $2^J$  where  $J$  is the level of the DWT decomposition. Second, the time step of the wavelet vector  $W_j$  is  $dt2^j$ , which may not correspond to the time when some interesting phenomenon is visible on the original time series. Third, when we circularly shift the time series, the corresponding wavelet coefficients, details and smooths are not a circularly shifted version of the wavelet coefficients, details and smooths of the original time series. Thus, the values of the wavelet coefficients, details and smooths are strongly dependent on the time when we start experimentally gathering the data. Finally, when we filter the time series to obtain the details and smooths, we introduce a phase shift, which makes difficult to line up meaningfully the features of the MRA with the original time series.

This is why we use instead the Maximal Overlap Discrete Wavelet Transform (MODWT). The MODWT transforms the time series  $X_t$  ( $t = 0, \dots, N - 1$ ) into  $J$  wavelet vectors  $\tilde{W}_j$  ( $j = 1, \dots, J$ ) of length  $N$  and a scaling vector  $\tilde{V}_J$  of length  $N$ . As is the case for the DWT, each wavelet vector  $\tilde{W}_j$  is associated with changes on scale  $\tau_j = dt2^{j-1}$ , and corresponds to the filtering of the original time series with a filter with nominal frequency interval  $[\frac{1}{dt2^{j+1}}; \frac{1}{dt2^j}]$ . The scaling vector  $\tilde{V}_J$  is associated with averages in scale  $\lambda_J = dt2^J$ , and corresponds to the filtering of the original time series with a filter with nominal frequency interval  $[0; \frac{1}{dt2^{j+1}}]$ . As is the case for the DWT, we can write the MRA:

$$X = \sum_{j=1}^J \tilde{D}_j + \tilde{S}_J \quad (2)$$

The MODWT of a time series can be defined for any length  $N$ . The time step of the wavelet vectors  $\tilde{W}_j$  and the scaling vector  $\tilde{V}_J$  is equal to the time step of the original time series. When we circularly shift the time series, the corresponding wavelet vectors, scaling vector, details and smooths are shifted by the same amount. The details and smooths are associated with a zero phase filter, making it easy to line up meaningfully the features of the MRA with the original time series. The wavelet methods for time series analysis are explained in a more detailed way in Percival and Walden (2000)).

### 3.2 Application to synthetic data

To illustrate the wavelet transform method, we first apply the MODWT to synthetics data. As slow slip events occur in Cascadia on a regular basis, every twelve to eighteen months, we create a synthetic signal of period  $T = 500$  days. To reproduce the ground displacement observed on the longitudinal component of GPS stations in Cascadia, we divide each period into two parts: In the first part of duration  $T-N$ , the displacement is linearly increasing and corresponds to the secular plate motion in the eastern direction; in the second part of duration  $N$ , the displacement is linearly decreasing and corresponds to a slow slip event on a reverse fault at depth triggering a ground displacement in the western direction. To see the effect of the magnitude of the slow slip event, we use different values for  $N = 2, 5, 10, 20$  days. Figure 1 shows the synthetics, the details of the wavelet decomposition for levels 1 to 8, and the smooth for the four durations of a slow slip event.

The ramp-like signal is transformed through the wavelet filtering into a waveform with first a positive peak and then a negative peak. The width of the waveform increases with the scale level. For the 8th level of the wavelet decomposition, the width of the waveform is nearly as large as the time between two events. We do not show details at larger scales as the corresponding waveforms would start to merge two contiguous events to-

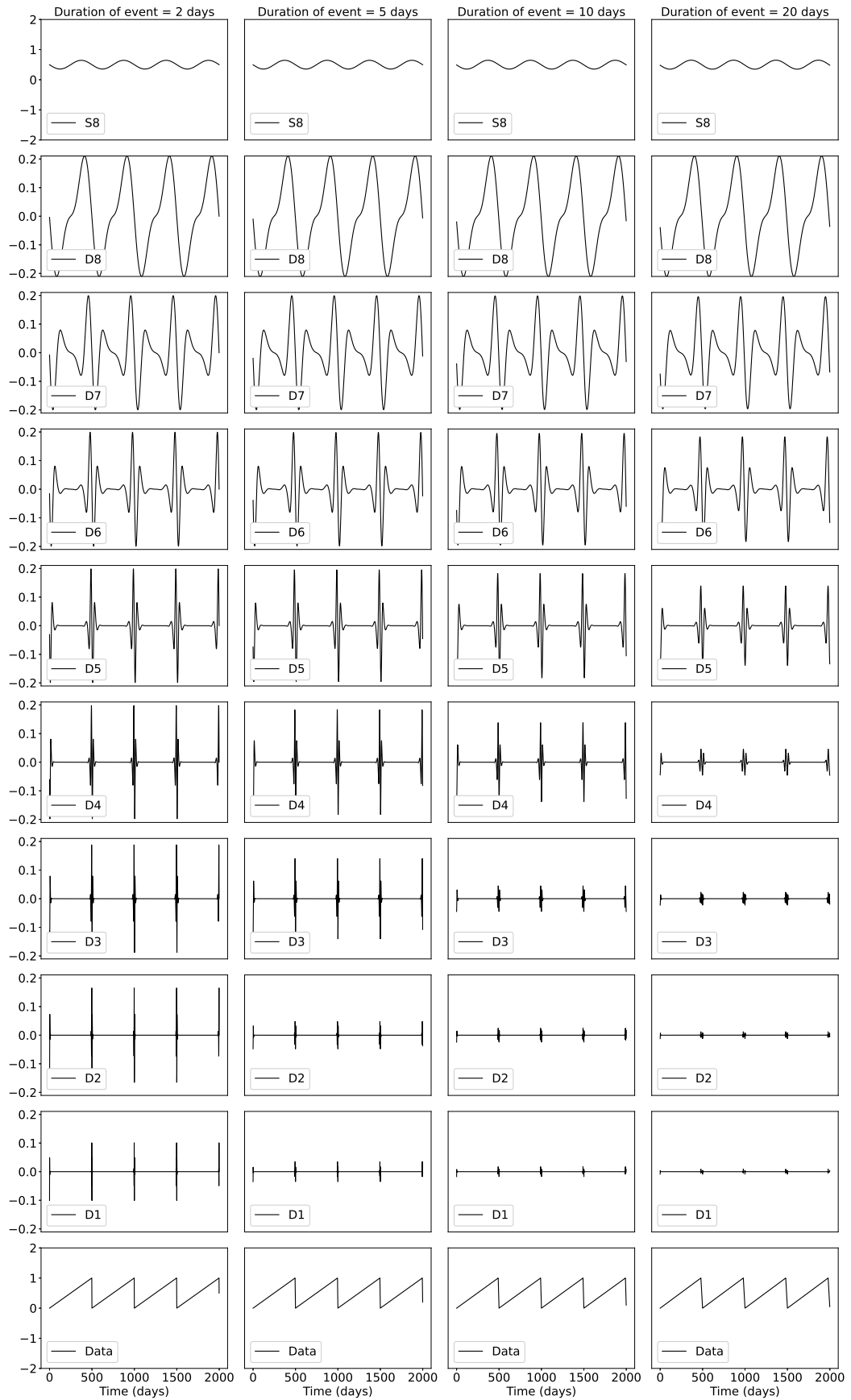


**Figure 1.** Details and smooth of the wavelet decomposition of a synthetics signal with period 500 days and duration of the slow slip event equal to 2 days (left), 5 days, 10 days, and 20 days (right).

209 gether, and make the wavelet decomposition less interpretable. For an event of duration  
 210 2 days, the wavelet details at levels higher than 2 have a larger amplitude than the wavelet  
 211 detail at level 1. For an event of duration 5 days, the wavelet details at levels higher than  
 212 3 have a larger amplitude than the wavelet details at lower scales. For an event of du-  
 213 ration 10 days, the wavelet details at levels higher than 5 have a larger amplitude than  
 214 the wavelet details at lower scales. For an event of duration 20 days, the wavelet details  
 215 at levels higher than 6 have a larger amplitude than the wavelet details at lower scales.  
 216 Thus, the scale levels at which an event is being seen in the wavelet details give us an  
 217 indication about the duration (and the magnitude) of the slow slip event. We expect the  
 218 big slow slip events of magnitude 6-7 that lasts about 10 days to start being visible at  
 219 the level 5 of the wavelet decomposition, but to not be noticeable at lower time scales.

### 220 3.3 MODWT of GPS and tremor data

221 The DWT and MODWT methods must be used on a continuous time series, with-  
 222 out gaps in the recordings. To deal with the gaps in the GNSS recordings, we simply re-  
 223 place the missing values by Gaussian noise with mean zero and standard deviation equal  
 224 to the standard deviation of the whole time series. We verify how the wavelet details may  
 225 be affected by looking at a GPS time series without missing values and comparing the  
 226 wavelet details with and without removing some data points. Station PGC5 has recorded  
 227 during 1390 days between 2009 and 2013, without any missing values. We first computed  
 228 the wavelet details without missing values. Then, we removed ten neighboring missing  
 229 values, replaced them by Gaussian noise, and computed the wavelet details with the re-  
 230 placed values. Figure 2 shows a comparison of the two wavelet details for two different  
 231 locations of the missing values. We can see that there are visible differences in the time  
 232 series itself, and in the details at the smallest levels of the wavelet decomposition. How-  
 233 ever, the differences between the wavelet details with and without missing values get smaller  
 234 and smaller with increasing levels the details, and are barely visible for the levels we are  
 235 mostly interested in (levels 6 to 8). We thus conclude that we can easily replace the miss-  
 236 ing values in the GNSS time series without introducing false detections of slow slip events.

237 We then applied the wavelet filtering to real GPS data. Figure 3 shows the longi-  
 238 tudinal displacement for GPS station PGC5, located in southern Vancouver Island, the  
 239 details of the wavelet decomposition for levels 1 to 8, and the smooth. In the data, we  
 240 can see a sharp drop in displacement whenever there is a slow slip event. For levels 5 to  
 241 8, we can see in the details a positive peak followed by a negative peak whenever there  
 242 is a drop in displacement in the data. We thus verify that the wavelet method can de-  
 243 tect slow slip events.

244 To increase the signal-to-noise ratio and be able to better detect slow slip events,  
 245 we stack the signal over several GPS stations. We choose to focus on GPS stations lo-  
 246 cated close enough to the tremor zone to get a sufficiently high amplitude of the slow  
 247 slip signal. We choose 16 points located on the 40 km depth contour of the plate bound-  
 248 ary (model from Preston, Creager, Crosson, Brocher, and Trehu (2003)) with spacing  
 249 equal 0.1 degree in latitude (red triangles on Figure 4). Then we took all the GPS sta-  
 250 tions located in a 50 km radius for a given point, compute the wavelet details for the lon-  
 251 gitudinal displacement of each station, and stack each detail over the GPS stations. We  
 252 thus have a stacked detail for each level 1 to 8 of the wavelet decomposition.

253 To compare slow slip events detected with GPS data and slow slip events detected  
 254 with seismic data, we took all the tremor epicenters located within a 50 km radius cen-  
 255 tered on one of the 16 locations marked by red triangles on Figure 3. Then we computed  
 256 the cumulative number of tremor within this circle. Finally, we removed a linear trend  
 257 from the cumulative tremor count, and applied the wavelet transform. Figure 5 shows  
 258 an example of the wavelet decomposition for the third northernmost location on Figure  
 259 4 (which is closest to GPS station PGC5). Contrary to what happens for the GPS data,  
 260 we see a sharp increase in the data whenever there is a tremor episode, which translates  
 261 into a negative peak followed by a positive peak in the wavelet details.

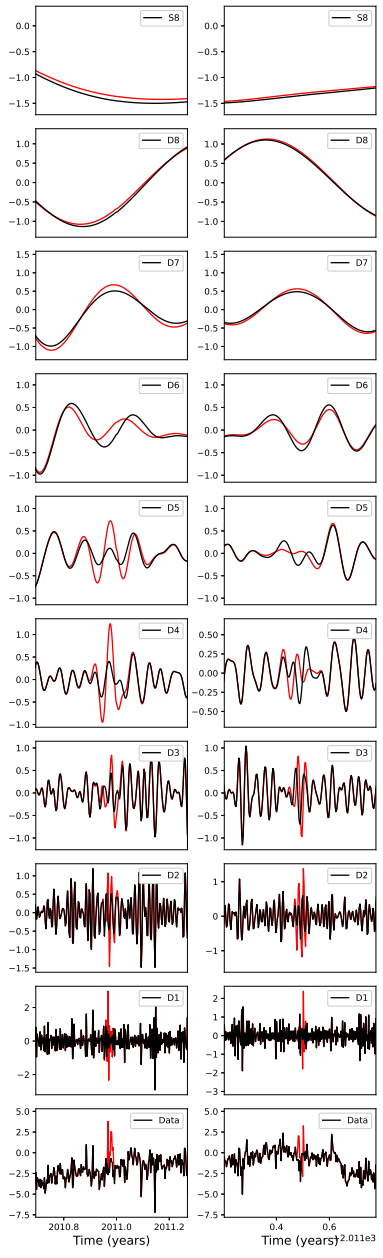


**Figure 2.** Bottom: Data from GPS station PGC5 without missing values (black) and with missing values replaced by Gaussian noise (red) for two locations of the missing values (left and right). Bottom to top: Corresponding eight details and smooths of the wavelet composition for the original data (black) and for the missing values replaced by Gaussian noise (red).

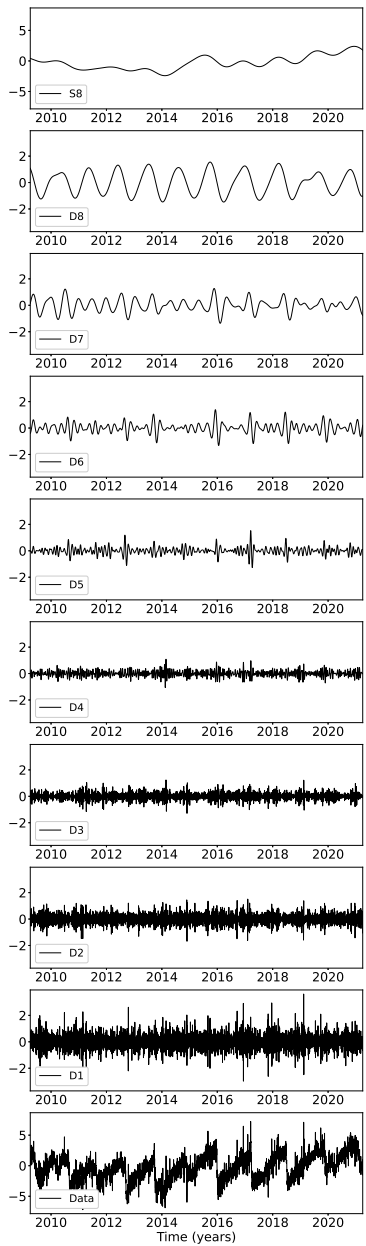


**Figure 3.** Details and smooth of the wavelet decomposition of the longitudinal displacement recorded at GPS station PGC5.

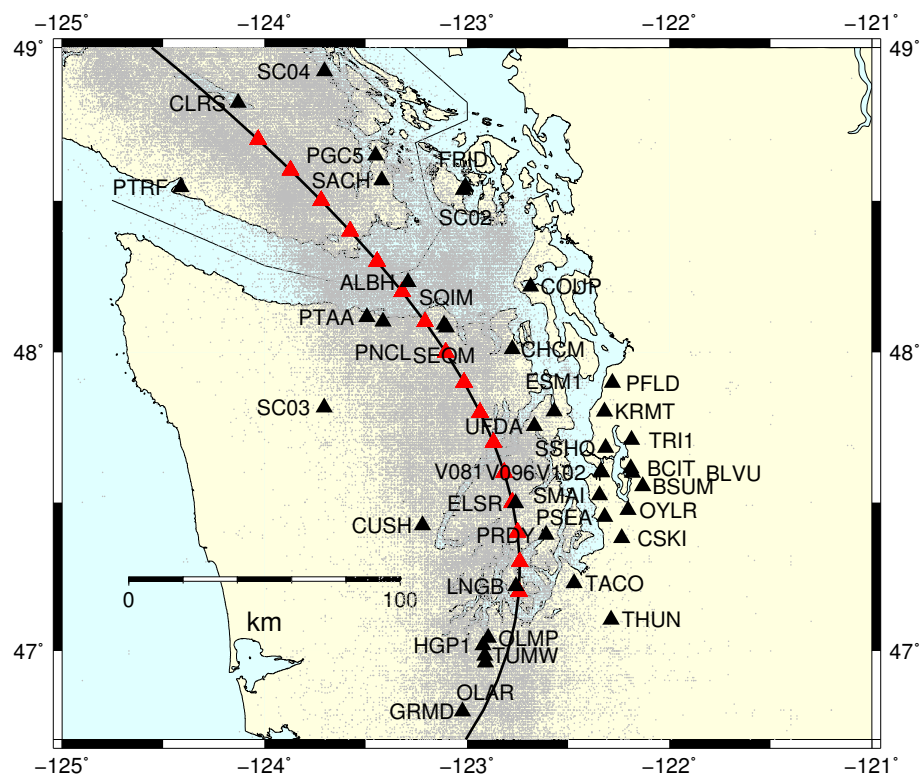


**Figure 4.** GPS stations used in this study (black triangles). The black line represents the 40 km depth contour of the plate boundary model by Preston et al. (2003). The red triangles are the locations where we stack the GPS data. The small grey dots are all the tremor locations from the PNSN catalog.

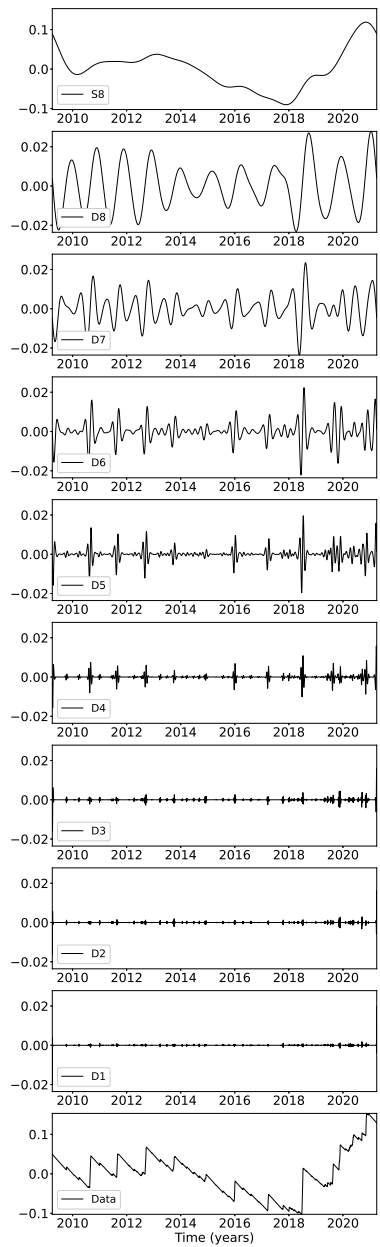


**Figure 5.** Details and smooth of the wavelet decomposition of the detrended cumulative tremor count around the third northernmost location on Figure 3.

262 **4 Results**

263 We stacked the 8th level detail of the wavelet decomposition of the displacement  
 264 over all the GPS stations located in a 50 km radius of a given point, for the 16 locations  
 265 indicated in Figure 3. The result is shown in the top panel of Figure 6, where each line  
 266 represents one of the locations. To better highlight the peaks in the wavelet details, we  
 267 highlighted in red the time intervals where the amplitude of the stacked detail is higher  
 268 than a threshold, and in blue the time intervals where the amplitude of the stacked de-  
 269 tail is lower than minus the threshold. To compare the GPS signal with the tremor sig-  
 270 nal, we plotted the 8th level detail of the wavelet decomposition of the tremor count on  
 271 the bottom panel of Figure 6. We used the opposite of the cumulative tremor count for  
 272 the wavelet decomposition in order to be able to match positive peaks with positive peaks  
 273 and negative peaks with negative peaks. Although the latitudinal extension of the events  
 274 is not always the same for the GPS data and for the tremor data, we identify the same  
 275 10 events in both 8th wavelet decompositions for the 8th level: Summer 2010, Summer  
 276 2011, Summer 2012, Fall 2013, Summer-Fall 2014, Winter 2015-2016, Winter 2017, Spring  
 277 2018, Spring-Fall 2019, and Fall 2020 - Winter 2021. We can also see the end of an 11th  
 278 event in Summer 2009.

279 Figures 7 and 8 show the same comparison between the wavelet decomposition of  
 280 the GPS data and the wavelet decomposition of the tremor count data for the 7th level  
 281 and the 6th level respectively. For the 7th level, we see the same events as for the 8th  
 282 level, both for the GPS data and the tremor count data. The wavelet decomposition is  
 283 more noisy for the GPS data in the earliest part of the time series, between 2010 and  
 284 2013, but it does not seem that there are more slow slip events visible in the 7th level.

285 For the 6th level detail, we see an additional event in Fall 2009 that is present both  
 286 in the GPS and the tremor data. There are three small signals in the GPS data in Spring  
 287 2012, Fall 2017, and Winter 2020 that are not present in the tremor data, and are prob-  
 288 ably false detections. To summarize, all the 11 events present on the 7th and 8th level  
 289 details of the wavelet decomposition are true detections, 12 of the 15 events present on  
 290 the 6th level detail of the wavelet decomposition are true detections.

291 **5 Discussion**

292 In addition to the magnitude 6 events discussed above, Michel, Gualandi, and Avouac  
 293 (2019) have also identified several magnitude 5 events using a variational Bayesian In-  
 294 dependent Component Analysis (vbICA) decomposition of the signal. As we expect smaller  
 295 magnitude events to be more visible at smaller time scales of the wavelet decomposi-  
 296 tion (levels 4 and 5), we verify for all these events whether a signal can be seen at the same  
 297 time as the time given in their catalog. Most of these magnitude 5 events are also sub-  
 298 events of bigger magnitude 6 events. Table 1 summarizes for each event its number as  
 299 indicated in the catalog from Michel et al. (2019), the beginning and end times as in-  
 300 dicated in the catalog from Michel et al. (2019), whether it is visible at the level 4 of  
 301 the wavelet decomposition, whether it is visible at the level 5 of the wavelet decompo-  
 302 sition, and whether it is part of a bigger magnitude 6 event. All 10 events that are sub-  
 303 event of a bigger event are visible at both levels 4 and 5. However, this may be due be-  
 304 cause the bigger event is in at levels 6 to 8, and also at smaller time scales. For the 3  
 305 small events that are not part of a bigger event, only one is visible at both time scales,  
 306 the other two are visible either for level either for level 5 of the wavelet decomposition.  
 307 Therefore, it is difficult to conclude whether the method can indeed detect events of mag-  
 308 nitude 5.

309 **6 Conclusion**

310 **Acknowledgments**

311 Enter acknowledgments, including your data availability statement, here.

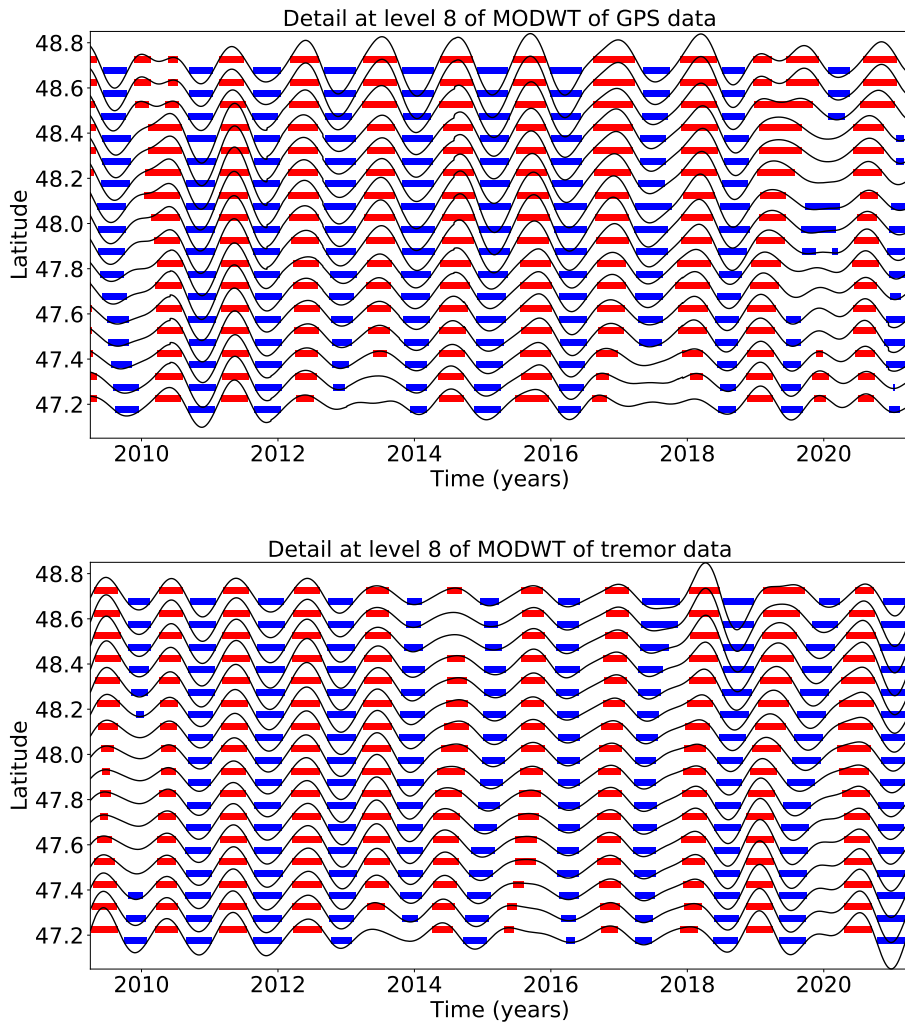


**Figure 6.** Top: Stacked 8th level details of the wavelet decomposition of the displacement over all the GPS stations located in a 50 km radius of a given point, for the 16 locations indicated in Figure 3. Bottom: Opposite of the 8th level detail of the cumulative tremor count in a 50 km radius of a given point for the same 16 locations.

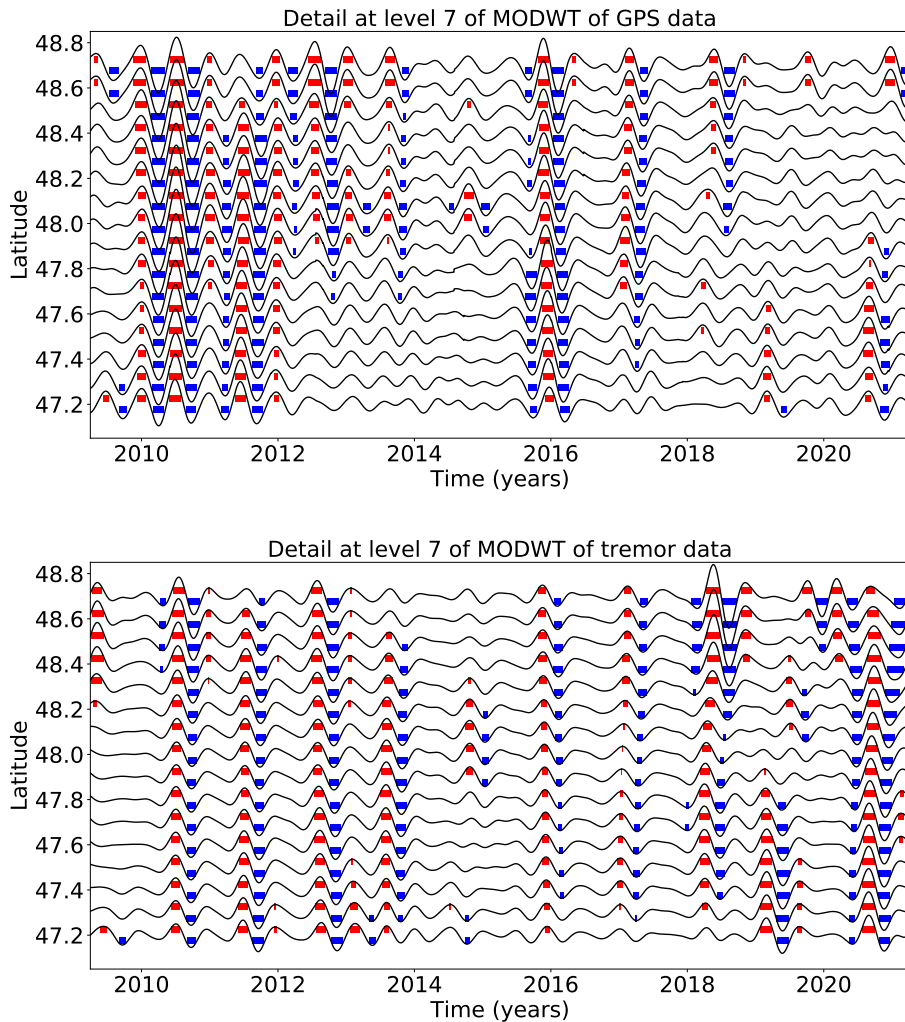


**Figure 7.** Top: Stacked 7th level details of the wavelet decomposition of the displacement over all the GPS stations located in a 50 km radius of a given point, for the 16 locations indicated in Figure 3. Bottom: Opposite of the 7th level detail of the cumulative tremor count in a 50 km radius of a given point for the same 16 locations.

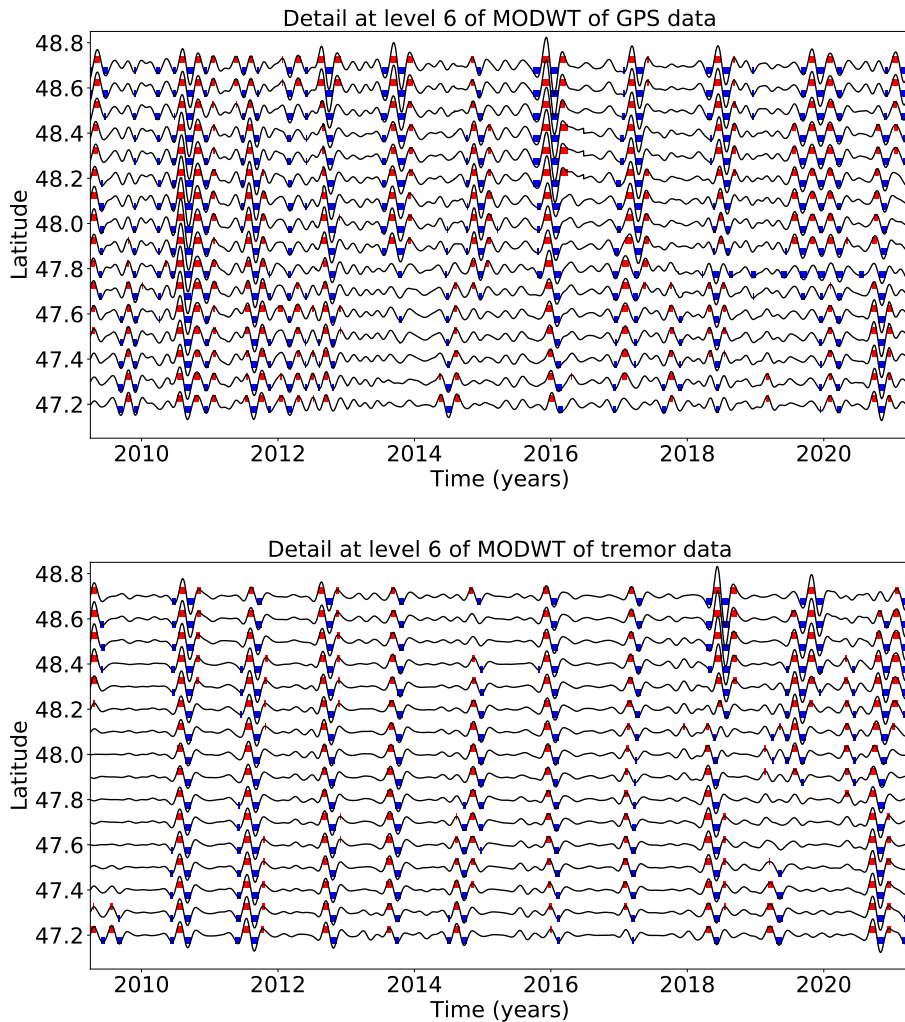


**Figure 8.** Top: Stacked 6th level details of the wavelet decomposition of the displacement over all the GPS stations located in a 50 km radius of a given point, for the 16 locations indicated in Figure 3. Bottom: Opposite of the 6th level detail of the cumulative tremor count in a 50 km radius of a given point for the same 16 locations.

**Table 1.** Magnitude 5 events from Michel et al. (2019).

Event number	Time	Visible at level 4	Visible at level 5	Sub-event of bigger event
25	2010.62-2010.67	Yes	Yes	Yes
29	2011.42-2011.45	No	Yes	No
31	2011.62-2011.68	Yes	Yes	Yes
32	2011.65-2011.68	Yes	Yes	Yes
35	2012.66-2012.72	Yes	Yes	Yes
42	2013.70-2013.78	Yes	Yes	Yes
44	2014.12-2014.20	Yes	No	No
45	2014.40-2014.48	Yes	Yes	No
49	2014.66-2014.71	Yes	Yes	Yes
52	2014.91-2014.95	Yes	Yes	Yes
57	2015.98-2016.08	Yes	Yes	Yes
60	2017.11-2017.15	Yes	Yes	Yes
61	2017.20-2017.24	Yes	Yes	Yes

## 312 References

- 313 Aguiar, A., Melbourne, T., & Scrivner, C. (2009). Moment release rate of Cascadia  
 tremor constrained by GPS. *Journal of Geophysical Research*, 114, B00A05.
- 314 Alba, S., Weldon, R. J., Livelybrooks, D., & Schmidt, D. A. (2019). Cascadia ETS  
 315 events seen in tidal records (1980–2011). *Bulletin of the Seismological Society  
 316 of America*.
- 317 Audet, P., & Kim, Y. (2016). Teleseismic constraints on the geological environment of deep episodic slow earthquakes in subduction zone forearcs: A review.  
 318 *Tectonophysics*, 670, 1-15.
- 319 Beroza, G., & Ide, S. (2011). Slow earthquakes and nonvolcanic tremor. *Annual Re-  
 320 view of Earth and Planetary Sciences*, 39, 271-296.
- 321 Frank, W. (2016). Slow slip hidden in the noise: The intermittence of tectonic re-  
 322 lease. *Geophysical Research Letters*, 43, 10125-10133.
- 323 Kumar, P., & Foufoula-Georgiou, E. (1997). Wavelet analysis for geophysical appli-  
 324 cations. *Reviews of Geophysics*, 35(4), 385-412.
- 325 Michel, S., Gualandi, A., & Avouac, J.-P. (2019). Interseismic coupling and slow slip  
 326 events on the Cascadia megathrust. *Pure and Applied Geophysics*, 176, 3867-  
 327 3891.
- 328 Obara, K. (2002). Nonvolcanic deep tremor associated with subduction in southwest  
 329 Japan. *Science*, 296(5573), 1679-1681.
- 330 Ohtani, R., McGuire, J., & Segall, P. (2010). Network strain filter: A new tool for  
 331 monitoring and detecting transient deformation signals in GPS arrays. *Journal  
 332 of Geophysical Research*, 115, B12418.
- 333 Percival, D., & Walden, A. (2000). *Wavelet Methods for Time Series Analysis*. New  
 334 York, NY, USA: Cambridge University Press.
- 335 Preston, L., Creager, K., Crosson, R., Brocher, T., & Trehu, A. (2003). Intraslab  
 336 earthquakes: Dehydration of the Cascadia slab. *Science*, 302, 1197-1200.
- 337 Rogers, G., & Dragert, H. (2003). Tremor and slip on the Cascadia subduction zone:  
 338 The chatter of silent slip. *Science*, 300(5627), 1942-1943.
- 339 Shelly, D., Beroza, G., & Ide, S. (2007). Non-volcanic tremor and low-frequency  
 340 earthquake swarms. *Nature*, 446, 305-307.
- 341 Szeliga, W., Melbourne, T., Miller, M., & Santillan, V. (2004). Southern Cascadia  
 342 episodic slow earthquakes. *Geophysical Research Letters*, 31, L16602.
- 343 Szeliga, W., Melbourne, T., Santillan, M., & Miller, M. (2008). GPS constraints on  
 344

- 346        34 slow slip events within the Cascadia subduction zone, 1997-2005. *Journal of*  
347        *Geophysical Research*, 113, B04404.
- 348        Wech, A. (2010). Interactive tremor monitoring. *Seismological Research Letters*,  
349        81(4), 664-669.
- 350        Wei, M., McGuire, J., & Richardson, E. (2012). A slow slip event in the south cen-  
351        tral Alaska Subduction Zone. *Geophysical Research Letters*, 39, L15309.